Physica Scripta. Vol. 39, 447–457, 1989.

Semiempirical Confrontations Between Theory and Experiment in Highly Ionised Complex Atoms*

Lorenzo J. Curtis

Department of Physics and Astronomy, University of Toledo, Toledo OH 43606, USA

Received July 1, 1988; accepted August 10, 1988

Abstract

Highly ionised complex atoms, which have many electrons stripped away but many electrons still remaining, are presently a subject of vigorous experimental study. The high precision experimentally attainable for these systems suggests their use in the investigation of higher order theoretical processes, and the specification of these interactions is essential to the development of reliable predictive methods. It is shown that parametric reductions which combine ab initio theoretical calculations with experimental observations can yield predictions of much higher precision than could be obtained from either source separately. These formulations also reveal subtle regularities in the measured data that are not exhibited by the corresponding computations, which suggest possible calculational improvements.

1. Introduction

There is much current experimental activity in the study of highly ionised complex atoms, which have both many electrons stripped away and many electrons still remaining. High precision measurements of the wavelengths and transition probabilities for these systems have been aided by the development of light sources utilising fast ion beams as well as laser-, tokamak- and astrophysically-produced plasmas. These studies are motivated by critical needs, eg, to facilitate plasma diagnostics, to aid in the interpretation of astrophysical measurements, and to improve computational approaches to fundamental theory.

While complex atoms with a large central charge are often dismissed as "hydrogenlike," their precise theoretical specification provides special challenges. It is true that the gross energy of these systems is dominated by the central potential, and that the ratio of the electrostatic fine structure to the magnetic fine structure becomes small and approaches the case in neutral hydrogen. However, differential core screening can greatly alter the relative strengths of higher order interactions: the magnetic fine structure and relativistic shifts in penetrating orbitals become large; M1 and E2 decay rates grow relative to E1 rates, and can cause "forbidden" transitions to dominate over "allowed" transitions; quantum electrodynamic effects can become substantial; and nuclear size effects grow in importance. Deeply penetrating orbitals in a highly ionised complex atom probe the inner regions of the core where few screening electrons are interposed between the active electron and the nucleus, a situation similar to a heavy atom stripped down to one or two electrons. Although the theoretical specification of a highly stripped system is cleaner than that of a deeply penetrating orbital in a partially stripped system, the ease of production and spectroscopic precision attainable for the latter offers promise for the study of interactions that become important only at high Z.

The development and availability of supercomputer facilities, coupled with the existence of user-friendly atomic structure computer codes and large scale data banks, have made possible new approaches to atomic research and have altered traditional boundaries between experiment and theory. Theoretical calculations can now be performed routinely by experimentalists prior to and during measurements. However, the ease of access and simplicity of use of these resources can conceal shortcomings in their reliability. *Ab initio* codes cannot be expected to yield spectroscopic accuracies routinely for complex systems, and a data bank is only as reliable as the critical criteria employed in its compilation.

Semiempirical methods provide a means for investigating the accuracy and consistency of theoretical and experimental results. They provide a sensitive exposition of deviations from simple models, and can yield predictive regularities and often reveal unsuspected linearities. Unfortunately these methods sometimes tend to fragment rather than to unify, since gross structure, fine structure, direct and exchange Slater energies, transition probabilities, etc, are each described by a separate and distinct parametrisation which emphasizes a particular region of the wave function. However, there are cases in which parameters deduced from the specification of one quantity can be directly utilised for the prediction of other quantities.

For these various reasons we have sought to develop systematic formulations that conjoin observations with computations on a very large scale, and to obtain predictions of higher reliability than could have been obtained from either approach separately.

2. Semiempirical and computational methods

The high precision requirements of atomic spectroscopy have, since the time of Janne Rydberg, been met through the use of semiempirical remappings of the observed data into a parametric space that amplifies subtle trends. This can be achieved by forcing many-body interactions to reside in an empirical parameter embedded in a quasi one-electron model. Examples of this approach [1] can be found in the quantum defect method, the Ritz expansion, the core polarization and core penetration models, and screening parametrisations. A spectral feature can be mapped into a corresponding quantity that is slowly varying along an isoelectronic, an isoionic, an isonuclear, or a homologous sequence or a Rydberg series, so as to reveal sensitive and

* This paper was originally presented at the workshop on "Frontiers in Atomic Structure Calculations and Spectroscopy" held at the University of Lund on 24–25 May 1988, and will be reprinted in the proceedings of that workshop.

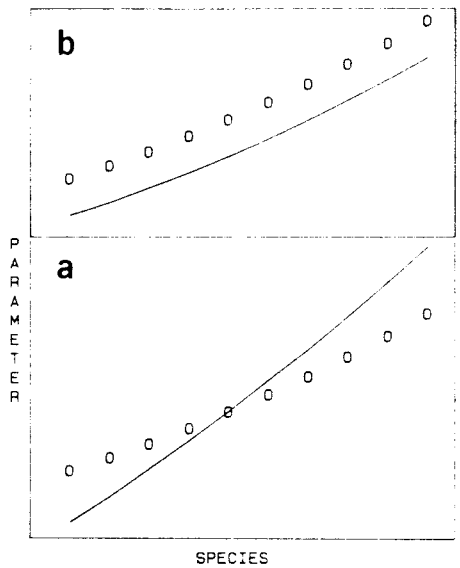

Fig. 1. Hypothetical confrontation between experimental data (circles) and theoretical models (solid lines) after reduction to a parameter that is slowly varying over a block of related data. Model (a) is correct for one ion, but predicts the wrong trend. Model (b) is nowhere correct, but predicts the correct trend.

subtle regularities or sudden departures from regularity that would otherwise go unnoticed.

This approach provides a number of advantages: it allows interpolations for missing data and extrapolations beyond the range of available measurements; it reveals misidentifications and questionable measurements; it allows blocks of related data to be smoothed, providing a data set with higher accuracy than that of any single data point; and it is a sensitive indicator of perturbing influences. Quantities sensitive to the inner portion of the wave function are often described by a parametrisation that multiplicatively scales its radial coordinates (such as a screening parametrisation), whereas quantities sensitive to the outer portion of the wave function are better described by a parameter that additively shifts its phase, such as the quantum defect.

The ability to perform *ab initio* calculations for a quantity over large numbers of similar atomic systems makes the joint application of semiempirical parametrisations to observed and calculated data very appealing. This approach makes possible new evaluation criteria on agreement between large scale experimental and theoretical trends, rather than between isolated specific cases. An hypothetical example is shown in Fig. 1, which illustrates a possible operational definition for a "good" and a "bad" theoretical calculation. Figure 1(a) presents a theoretical model that predicts an erroneous trend, but crosses the experimental data for a specific atomic species where it yields local apparent agreement. Figure 1(b) shows an alternative model that reproduces the trend of the observed data with a constant discrepancy, so that it does not yield the correct result for any atomic species. Clearly the theory of Fig. 1b could be empirically shifted to coincide with the observed data, and yield highly precise predictions. Using the criterion proposed here, the theory of Fig. 1(b) would be judged superior to that of Fig. 1(a). (Metaphorically, a stopped clock is correct twice a day; a clock that runs one hour fast is always wrong but can be used as a timepiece.)

In several studies described below, existing spectroscopic data are compared with multiconfiguration Dirac–Fock calculations that were performed specifically for this purpose using the program MCDF developed by Grant and coworkers [2]. These calculations were carried out by network using the MFE Cray X-MP computer in Livermore California. Other supporting calculations were made using the NAS 9080 and VAX 785 computers at the University of Toledo.

3. Screening parameter reductions of J dependent splittings

The J-dependent energy splitting within a spectral term is often determined to much higher experimental precision than is possible for the gross energy or for other splittings. Most theoretical approaches seek wave functions that optimise the prediction of the gross energy (arising primarily from the $1/r$ central Coulomb potential), and treat interactions that fall off more steeply with r perturbatively. Consequently, some of the most precisely measured spectroscopic data are primarily sensitive to the portion of the wave function that is least well specified by standard theoretical methods. Therefore, it should not be surprising that semiempirical studies of J-dependent fine structure reveal regularities, linearities, and discontinuities that are not predicted by *ab initio* theories.

The screening parameter approach has been applied to spectroscopic data since the time of Arnold Sommerfeld, but modern developments have made it possible to generalise and extend its usage. This approach, historically known as the regular doublet law, defines a screening parameter S by forcing equality between a measured interval in an atom of central charge Z and the corresponding interval in a fictional hydrogen-like atom of the same quantum numbers and a central charge $Z - S$. As an example, consider the formulation for a p-state spin–orbit energy ζ_{np}. To generalise slightly from the one electron case, we shall treat cases where several valence electrons all have the same principal quantum number n, and have orbital angular momenta that sum to $L = 1$. For compactness, we incorporate the fine structure constant α into the effective screened charge, which we denote by

$$x = \alpha(Z - S). \tag{1}$$

The hydrogen-like expression for this system is

$$\zeta_{np} = \frac{R\alpha^2 x^4}{3n^3}\left[(1 + F_{\mathrm{SD}})(1 + m/M) + F_{\mathrm{QED}} + F_{\mathrm{RM}} + F_{\mathrm{NP}}\right] \tag{2}$$

Here, F_{SD} represents higher order corrections in the Sommerfeld expansion of the Dirac energy, which are given by

$$F_{\mathrm{SD}} = \sum_{i=1}^{I} x^{2i} \sum_{k=0}^{2i} n^{k-2i}(2 - 2^{-k})C_{ik} \tag{3}$$

where the C_{ik} are a set of rational fractions tabulated to 18th order in Ref. [3]. Next, F_{QED} denotes the self-energy corrections (discussed in Section 5) which can be represented by the explicit expression [4]

$$\begin{aligned} F_{\mathrm{QED}} = {} & g - 2 - \frac{3\alpha}{4}x^3 + \frac{4\alpha}{3\pi}(1 - n^{-2}) \\ & \times (2\ln x - 11.24 + 7.476x^2)x^2 \\ & + (4\alpha/\pi)(0.0068 - 2.593x^4) \end{aligned} \tag{4}$$

Further, F_{RM} includes higher order corrections for the relativistic nonseparability of the reduced mass and for nuclear

Table I. *Breakdown of the contributions to the 4p fine structure in Cu-like Nd ($Z = 60$) as specified by eq. (1), expressed both in cm^{-1} and in gravitational heights above the surface of the earth*

Phenomenological origin	Energy level contribution	Earth's gravity analogue
Ionisation energy		
($4p$ cg)	9 282 570 cm^{-1}	6378 km
Sommerfeld fine structure		
4th order	244 292 cm^{-1}	168 km
6th order	18 808 cm^{-1}	13 km
8th order	1464 cm^{-1}	1 km
10th order	123 cm^{-1}	84 m
12th order	11 cm^{-1}	8 m
14th order	1 cm^{-1}	69 cm
16th order	0.1 cm^{-1}	7 cm
18th + order	0.01 cm^{-1}	7 mm
Quantum Electrodynamics		
g-2	567 cm^{-1}	390 m
higher order	−52 cm^{-1}	−36 m
Nuclear Recoil		
reduced mass	0.9 cm^{-1}	62 cm
higher order	−0.004 cm^{-1}	−3 mm
Nuclear Penetration	14 cm^{-1}	10 m

recoil effects. These two corrections are well understood only if treated separately [7] and many approaches yielding different suggested corrections can be found in the published literature [e.g., 5–9]. Fortunately, this correction is quite small, and a typical formulation [7] yields

$$F_{RM} = -\frac{(m/M)^2}{(1 + m/M)^3} + \frac{\alpha/\pi}{(1 + m/M)^2} - \alpha/\pi. \quad (5)$$

Finally, F_{NP} accounts for nuclear penetration, which has been shown [10] to be significant for high Z members of this sequence. An approximation formula has been obtained [11] based on MCDF computations of the Z dependence of these corrections, obtained using uniform sphere and Thomas–Fermi models for the nuclear charge distribution. The expression below was obtained using $n = 4$, but the result was only weakly dependent upon principal quantum number.

$$F_{NP} = 2.7\alpha^3(1 - 2.1x^4)\exp(11.1x). \quad (6)$$

The screening parametrisation is achieved by inverting eq. (2) (by numerical iteration), thus mapping each measured ζ_{np} into a corresponding value for S. When studied isoelectronically, S has been found to be highly regular as a function of the reciprocal effective central charge, often accurately represented by the linear relationship

$$S = a + b/(Z - S). \quad (7)$$

Although the detail contained in the corrections of eqs. (3–6) may seem excessive in view of the empirical nature of the formulation, studies described below indicate that the inclusion of these higher order corrections produces a set of screening parameters of greater isoelectronic regularity, and thus of greater predictive power. Furthermore, similar semiempirical representations of these higher order effects are routinely included as options in commonly-used *ab initio* codes.

To further emphasize the significance of including these seemingly small effects, a breakdown of the contributions to the $4p$ fine structure of Cu-like Nd^{31+} ($Z = 60$) is given in Table I, and scaled to analogous gravitational potentials

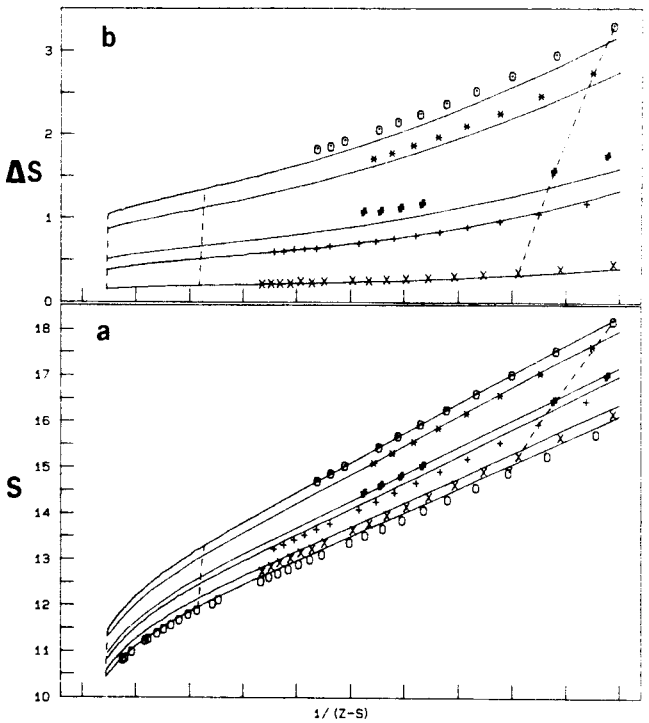

Fig. 2. Parametric reduction of ζ_{nl} for the $4s^x4p^{y\ 1,3}P$ terms in the Cu(○), Zn(×), Ga(+), Ge(#), Se(*) and Br(⊙) isoelectronic sequences. Symbols denote experimental observations, solid lines trace MCDF calculations, and dashed lines connect ions with $Z = 35$, 60 and 92 across the sequences. Fig. 2(a) plots the screening parameter S versus the reciprocal screened charge $1/(Z - S)$. Fig. 2(b) plots the differential screening parameters $S - S(\mathrm{Cu})$ for the multiple valence electron systems relative to that for the Cu sequence vs the same abscissa.

at the surface of the earth. The Nd energy contributions were obtained by reducing the measured fs interval [12] (265 110 cm^{-1}) to the corresponding screening parameter ($S = 11.9$) using eqs. (2–6), and then evaluating each of its separate contributions. The ionisation energy of the $4p$ level is the difference between the centroid of its measured excitation energies [12] and the experimental ionisation limit [12]. The gravitational problem can be written in terms of the radius r of the earth and the height h above its surface

$$\frac{GMm}{(r + h)} = \frac{GMm}{r}(1 - h/r + \ldots). \quad (8)$$

In this analogy, Table I equates h/r to the ratio of the Nd contribution to its ionisation energy. Notice that, for example, the neglect of nuclear penetration in the fs of Nd^{31+} is analogous to ignoring a fall off an olympic 10 meter diving board at sea level.

4. Applications to fs splittings in $ns^xnp^{y\ 1,3}P$ terms

An example of the application of this method to fine structures of the lowest lying P terms in the Cu, Zn, Ga, Ge, Se and Br isoelectronic sequences is shown in Fig. 2(a). The dominant configurations for these systems consist of a closed $n = 3$ shell nickel core, with additional $4p$ (Cu), $4s4p$ (Zn), $4s^24p$ (Ga), $4s^24p^2$ (Ge), $4s^24p^4$ (Se) and $4s^24p^5$ (Br) valence electrons. (The half-filled $4p^3$ configuration of the As sequence has no linear dependence upon ζ_{np} and was omitted). The Cu, Ga and Br terms are doublets and yield ζ_{np} directly, as does the $J = 0$–2 interval of the Zn triplet. For the Ge and Se triplets, ζ_{np} and the Slater electrostatic energy F_2 were

Table II. *Positions of the 1s and 2p orbital turning points (in milli Bohr radii) obtained from a semiclassical self-consistent field calculation using position probability densities and the Einstein–Keller–Brillouin quantisation condition. The results of the nonrelativistic calculation are given in parentheses after the relativistic calculation. Notice that for the relativistic calculation the finite perihelion of the 1s (produced by the Maslov index) collapses at $Z = 1/2\alpha$, and that the 1s aphelion jumps inside the 2p perihelion somewhere between $Z = 54$ and 74*

	1s		2p	
Z	Perihelion	Aphelion	Perihelion	Aphelion
42	2.1 (3.2)	39 (45)	34 (35)	176 (179)
54	0.9 (2.5)	26 (35)	25 (26)	132 (134)
74	0 (1.8)	13 (25)	17 (19)	92 (96)

obtained from a reduction of the relative spacings of the ^3P levels alone, without recourse to the positions of the ^1S and ^1D levels.

In Fig. 2 character symbols represent experimental observations for the Cu (○) [12–15], Zn (×) [16–19], Ga (+) [20, 21], Ge (#) [22], Se (*) [22–24] and Br (⊙) [25] sequences, solid curves denote our MCDF calculations, and dashed lines trace isonuclear comparisons at $Z = 35$, 60 and 92. Although the agreement between theory and experiment is superficially good (to within a few percent) and seems to improve with increasing Z, there are systematic discrepancies on the level of the spectroscopic accuracies that characterise the data base. The tendency for the MCDF calculations to overestimate the screening is clear for the Cu, Zn and Ga sequences, and a crossing of the theoretical and experimental curves may be occurring for the Ge, Se, and Br sequences.

Least squares fits reveal that the observed data for the Cu sequence in the region $Z \leqslant 60$ (31 times ionised) have a high degree of linearity on this plot that is not present in the MCDF calculations. For $Z > 60$ there is a departure from this linearity producing a sharp discontinuity. This suggests a possible redistribution of charge in the inner core. The MCDF calculations exhibit a gentle curvature with no linear region and no discontinuity in slope.

Although no theoretical mechanisms for a redistribution of core charge near $Z = 60$ have been found, such mechanisms do exist in a semiclassical model that includes relativity. A semiclassical self-consistent field calculation has been performed [26] using position probability densities obtained from Kepler orbits quantised by the Einstein–Brillouin–Keller condition. When the relativistic equations for the kinetic energy are used in this formulation, two discontinuities occur in the vicinity of $Z = 60$ that are illustrated in Table II.

One discontinuity involves the topological Maslov index 1/2 that occurs in the EBK formulation. This causes S-states to have a small but finite perihelion for the nonrelativistic and low Z relativistic problems, but in the relativistic formulation this S-state perihelion collapses for $Z \geqslant 1/2\alpha = 68.5$ (a similar singularity at $Z = 1/2\alpha$ exists for the Klein–Gordon equation; for the Dirac equation the singularity occurs at $Z = 1/\alpha$).

A second discontinuity involves the isoelectronic variation of the positions of the 1s aphelion and the *np* perihelions. As can be seen from Table II, the 2p perihelion is inside the 1s aphelion for all values of Z in the nonrelativistic computation and for the relativistic calculations at $Z = 42$ and 54. However, for $Z = 74$ in the relativistic calculation the 2p orbit lies entirely outside that of the 1s. Although this shift in relative positions occurs somewhere in the vicinity of $Z = 60$, its precise position is sensitive to the initial trial charge distribution used in the self-consistent field calculation, and cannot be uniquely specified. For values of Z in this intermediate range, the relative positions of the *np* perihelions and the 1s aphelion tend to remain where they were initially placed. If an isoelectronic calculation is performed in which the charge distribution obtained for one value is Z is used as a starting value for the next lower (or higher) value of Z, this redistribution does not occur in a smooth isoelectronic manner, but rather as a sudden and discontinuous jump through a region of instability that depends on the direction that Z is incremented. This bifurcation causes irreproducible and possibly chaotic results in the relativistic semiclassical problem, but no similar effect seems to occur in either the nonrelativistic classical or the quantum mechanical problem.

The apparent linearity in the $Z \leqslant 60$ region of the Cu sequence provides a useful tool for evaluation and interpolation, and we have reported [11] an attempt to further enhance this linearity by empirical adjustment of the various small interaction terms in eq. (2). In this study, weighted least squares fits of eq. (7) to the reduced data were made using various models for the QED and nuclear penetration corrections in eq. (1), and the resulting chi-squared probabilities were examined. The QED corrections were made in three different ways: anomalous magnetic moment ($g - 2$) only; hydrogenlike Lamb shift with no screening; and hydrogenlike Lamb shift with the same screening as the fine structure. Each option was also performed with and without the nuclear penetration corrections. Based on the chi-squared test, the fs-screened Lamb shift was the best, followed by the bare g-2 model, and the unscreened Lamb shift was the worst of the three. Inclusion of the nuclear penetration corrections improved the fits slightly in all cases. There is presently no theoretical basis for this empirical linearity, and while it appears that QED and nuclear penetration effects are being probed by this analysis, it is also possible that these functional Z dependences merely mimic those of some other important interaction. Irrespective of such questions, these results demonstrate that semiempirical interpolations can be sharpened by including the functional representations for these higher order interactions in the mapping function of eq. (2).

The fine structures for the Cu sequence have been measured through Bi^{83+}, making it the most comprehensively known isoelectronic fs data set. By semiempirical methods, the extensive data available and the regularities revealed within the Cu sequence can be exploited [27] to yield precise predictions in more complex and less reliably calculable systems, such as the lowest lying P states in the Zn, Ga, Ge, Se and Br sequences. Despite the breakdown of the linearity in Fig. 2 at $Z = 60$, these systems can be precisely specified through the use of differential screening parameters.

Figure 2(b) presents a plot of the isonuclear difference between the screening parameter for each of the other five sequences and that of the Cu sequence, also plotted vs the

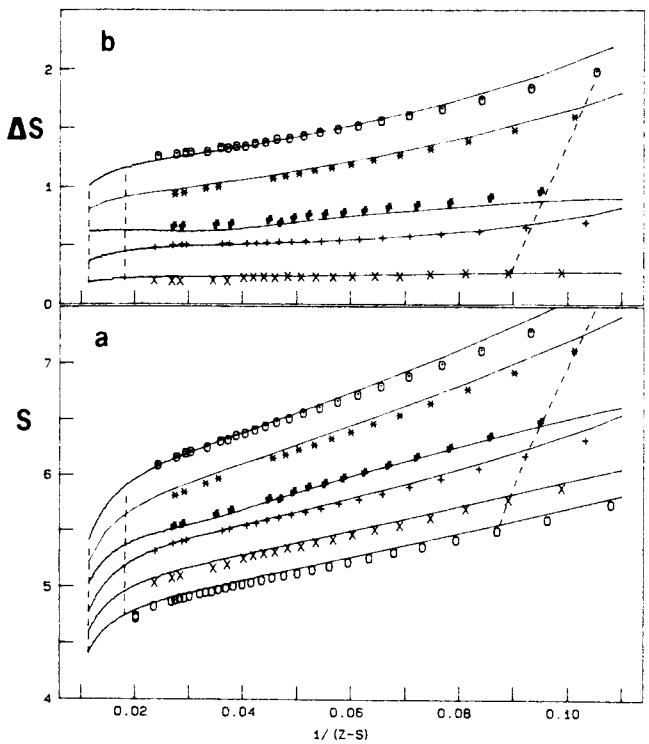

Fig. 3. Parametric reduction of ζ_{nl} for the $3s^2 3p^{1,3}P$ terms in the Na(○), Mg(×), Al(+), Si(#), S(*) and Cl(⊙) isoelectronic sequences. Symbols denote experimental observations, solid lines trace MCDF calculations, and dashed lines connect ions with Z = 17, 60 and 92 across the sequences. Fig. 3(a) plots the screening parameter S versus the reciprocal screened charge $1/(Z - S)$. Fig. 3(b) plots the differential screening parameters $S - S$(Na) for the multiple valence electron system relative to that for the Na sequence vs the same abscissa.

corresponding reciprocal screened charge. Although the curves are not linear on this plot, the MCDF results do not exhibit any discontinuity in slope at Z = 60. This suggests that the screening parameter can be decomposed into a dominant component due to the closed n = 3 core and a smaller component due to the n = 4 valence electrons. In addition, the observed values for Zn, Ga, Ge, Se and Br indicate that the MCDF calculations tend to overestimate this difference by an amount that is roughly constant for each sequence, permitting them to be empirically corrected as was illustrated in Fig. 1(b). Thus the core component of S can be accurately deduced from measurements in the Cu sequence and the out-of shell component can be theoretically computed and empirically adjusted using low Z data.

The screening parameter approach to the specification of J dependent splittings is applicable to ns^2np^1 systems with values of n other than 4, provided a sufficient base of measured data exists. Figures 3(a) and 3(b) present sets of screening parameter and differential screening plots (homologous to Fig. 2) for the Na, Mg, Al, Si, S and Cl sequences. The dominant configurations here consist of a closed n = 2 shell neon core, with additional $3p$ (Na), $3s3p$ (Mg), $3s^2 3p$ (Al), $3s^2 3p^2$ (Si), $3s^2 3p^4$ (S) and $3s^2 3p^5$ (Cl) valence electrons. Here the symbols represent observed data for the Na (○) [28–34], Mg (×) [35], Al (+) [36], Si (#) [37–40], S (*) [37–40] and Cl (⊙) [36] sequences.

Figure 3(a) indicates that here again there is a high Z downturn in the theoretical curves on this plot. On the basis of these experimental data, it appears that the discontinuity occurs at approximately the same stage of ionisation (31 times ionised) as in the Cu sequence, and not at the same nuclear charge (Z = 42 rather than Z = 60). Figure 3(b) shows that the high Z downturn is largely contained in the Na sequence data, and only a small effect appears in the difference between the individual screening parameters and the corresponding value for Na.

For multiple valence electron configurations, the constituent levels are specified by the spin–orbit operator and additional electrostatic operators (e.g., direct and exchange Slater energies), which can also be reduced to a screening parameter representation. For $nsnp$ configurations, screening parametrisations of the G_1 exchange Slater integral have been found [41] to exhibit linearity on an S vs $1/(Z - S)$ plot. For the ns^2np^2 and ns^2np^4 configurations, screening parametrisations of the direct Slater energy F_2 have also been carried out [42].

The methods described above permit large blocks of fine structure splittings to be predicted using high Z data from one sequence, low Z data for other sequences, and empirically adjusted ab initio calculations. This interweaving of data and computations illustrates the strength of the semiempirical approach to producing large scale compilations of precision atomic structure data.

5. Screening parametrisation of the self-energy corrections to the regular and irregular doublet laws

As described above, studies of the $4p$ fine structure in the Cu sequence indicated that the isoelectronic linearity of the screening parametrisation was improved if hydrogenlike QED self-energy corrections screened in the same way as the fine structure are included in the reduction formula of eq. (2). Screening of the hydrogenic Lamb shift in few electron atoms is currently an area of activity in ab initio theory, and this provides a test of the approach we have adopted for use in complex atoms. Precision calculations for the $2s\,^2S_{1/2}$–$2p\,^2P_{1/2}$ (irregular doublet) and the $2p\,^2P_{1/2}$–$2p\,^2P_{3/2}$ (regular doublet) intervals for the Li isoelectronic sequence have recently been performed by Johnson, Blundell and Sapirstein [43]. They have included all interactions except for the Lamb shift, and have shown that the residue between the observed intervals and their calculations exhibits substantial discrepancies with the corresponding unscreened hydrogen-like Lamb shift.

These calculations provide an excellent basis for precise predictions of these intervals, as is shown in Fig. 4. Here the empirical Lamb shifts for the regular and irregular doublets are obtained by subtracting the predictions of Ref. [43] from the corresponding observed data [44–49]. The effective screening parameter is obtained by forcing equality between this residue and the hydrogenic expression for the corresponding Lamb shift with an adjustable effective charge. In Fig. 4 the screening of the Lamb shift contribution to the $2s\,^2S_{1/2}$–$2p\,^2P_{1/2}$ interval is denoted by (×) and the screening of the Lamb shift contribution to the $2p\,^2P_{1/2}$–$2p\,^2P_{3/2}$ interval is denoted by (+). The screening parameter obtained from the Sommerfeld reduction of the total fine structure splitting (the n = 2 equivalent of eq. (2)) is also plotted in Fig. 4 for comparison, and is denoted by (○).

Predictions for the wavelengths of the resonance transitions in highly ionised members of the Li sequence can be obtained by extrapolating trends exhibited in Fig. 4, and adding the corresponding screened hydrogenlike Lamb shift

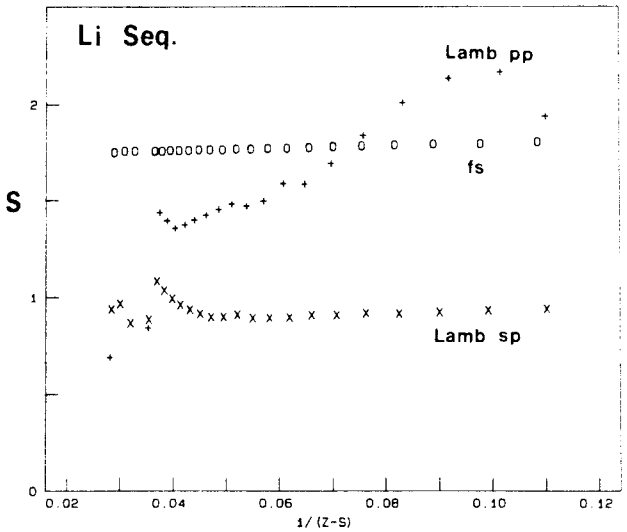

Fig. 4. Screening parametrisation of the empirical values for the Lamb shift for the $n = 2$ regular (+) and irregular doublets (×) in the Li isoelectronic sequence. Empirical Lamb shifts are given by differences between observed splittings and the calculations of Ref. [43]. The parametrisation is defined by a screened hydrogenic expression for the corresponding Lamb shift. For comparison, (O) traces a Sommerfeld screening parametrisation of the total fine structure.

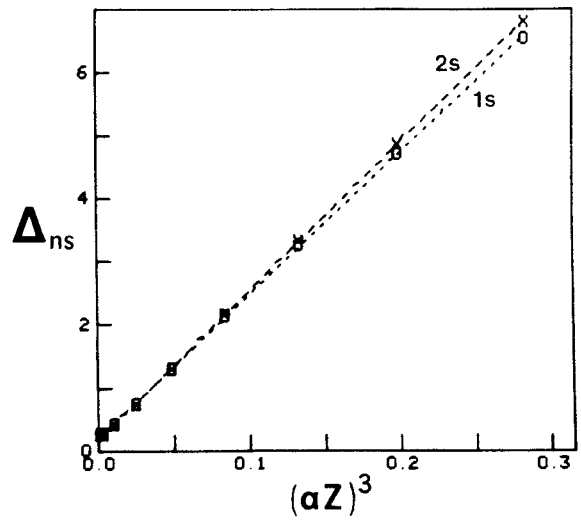

Fig. 5. Plot of the difference between numerical calculations [50, 51] and the perturbation expansion [5, 51] for the hydrogenlike Lamb shift for the 1*s* and 2*s* levels vs $(\alpha Z)^3$.

corrections to the *ab initio* calculations of Ref. [43]. As an example, Table III presents the results obtained by setting the empirical Lamb shift screening parameters $S(\text{irreg}) = 0.9$ and $S(\text{reg}) = 1.4$ for the irregular and regular doublet intervals. Table III also compares these predictions with recent measurements [45–49]. Clearly the accuracy of this method can be greatly improved as additional measurements of these intervals (perhaps aided by these predictions) become available.

Notice that all three screening parameters in Fig. 4 can be characterised at high Z by $S = 1.5 \pm 0.2$. This is consistent with the study [11] of small contributions to the $4p$ fine structure in the Cu sequence described above, which indicated that a hydrogenic expression for the Lamb shift that was screened in the same way as the fine structure produced better isoelectronic linearity in the parametrisation than either the unscreened or the bare g-2 model. While the Z dependences of the three screening parameters in Fig. 4 differ (and make their interchanged usage a "bad" theory by the criterion of Fig. 1) it is possible that these differences are diminished for the Cu sequence. Hydrogenic parametrisations are usually more successful in describing system with many-electron cores and high-n valence electrons, and thus tend to improve homologously.

To facilitate the use of screened hydrogenic expressions for QED self-energy corrections, explicit functional (albeit approximate) expressions such as eq. (4) are useful. To facilitate these semiempirical formulations, we have combined existing perturbation expansions [5, 51] with published exact numerical calculations [50, 51] and parametrised the difference. A number of interesting insights have been obtained in this manner [4].

Figure 5 displays on the same plot the differences between the exact calculations and the perturbation expansions for

Table III. *Predictions for Li sequence resonance transition wavelengths (in Å), obtained by adding screened hydrogen-like Lamb shift corrections to the ab initio calculations of Ref. [43]. From Fig. 4, empirical Lamb shift screening parameters $S(\text{irreg}) = 0.9$ and $S(\text{reg}) = 1.4$ were chosen for the irregular and regular doublet intervals. Results are compared with recent measurements (uncertainties in parentheses)*

Z Ion	λ ($3s$–$3p_{1/2}$) Pred.	Obs.	λ ($3s$–$3p_{3/2}$) Pred.	Obs.	Ref.
26 Fe 23+	255.125	255.11 (3)	192.037	192.05 (3)	[45]
27 Co 24+	244.239		178.225		
28 Ni 25+	234.159	234.140	165.411	165.396	[46]
29 Cu 26+	224.796	224.80	153.517	153.51	[47]
30 Zn 27+	216.073		142.474		
31 Ga 28+	207.923		132.222		
32 Ge 29+	200.292	200.30 (5)	122.707	122.73 (5)	[46]
33 As 30+	193.124		113.876		
34 Se 31+	186.386	186.36 (2)	105.686	105.70 (2)	[48]
35 Br 32+	180.040		98.092		
36 Kr 33+	174.040	174.025 (26)	91.052	91.040 (25)	[49]
37 Rb 34+	168.368		84.530		
38 Sr 35+	163.000		78.492		
39 Y 36+	157.901		72.901		
40 Zr 37+	153.042		67.722		
41 Nb 38+	148.400		62.925		
42 Mo 39+	143.986		58.489		

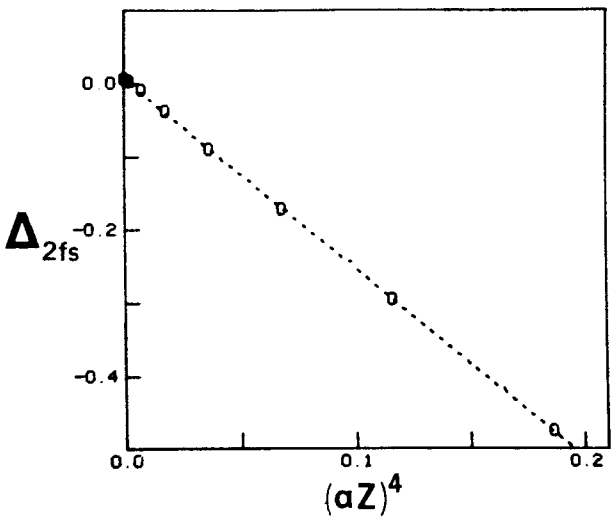

Fig. 6. Plot of the difference between numerical calculations [50, 51] and the perturbation expansion [5, 51] for the hydrogenlike Lamb shift for the $2p$ fine structure vs $(\alpha Z)^4$.

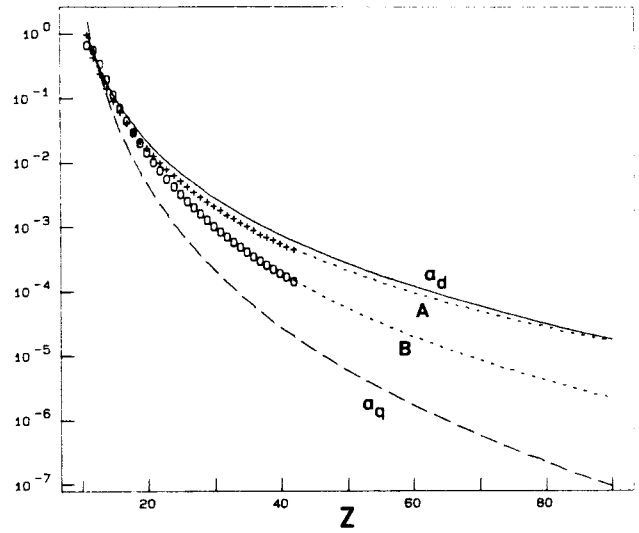

Fig. 7. Plot of the theoretical dipole and quadrupole polarisabilities α_d and α_q [52] for the Ne sequence and the effective experimental values A and B for these quantities obtained [53] from high Rydberg states in the Na sequence. The α_d values are traced by the solid line, the α_q values are traced by dashed line, the values for A are denoted by (+) and the values for B are denoted by (○). The extrapolation of A and B by the formulae of Edlén [53] are indicated by dotted lines.

both the $1s$ and $2s$ states, plotted vs $(\alpha Z)^3$. The plot is not only remarkably linear, but displays a surprising lack of dependence upon n. Figure 6 shows the difference between the exact and perturbation values for the Lamb shift in the fine structure splitting $2p$ $(^2P_{3/2}-^2P_{1/2})$ plotted vs $(\alpha Z)^4$, indicating a similarly linear exposition. Straight line fits of these quantities as a function of the plotting abscissae provide a convenient means for semiempirically modelling the core charge scaling of the self energy corrections for complex atoms, as well as a means of extrapolating these corrections to higher values of n than have yet been calculated by ab initio methods. The apparent linearity revealed on Figs. 5 and 6 also provides motivation for reexamining the perturbation expansion approach, to determine whether this is merely a conspiracy of interactions which mimic a straight line, or if there is a single physically interpretable interaction that dominates the charge dependence of this residue.

6. Core polarisabilities and ionisation potentials

For states of sufficiently high n and l the gross energy of the active electron and the passive core are coupled only through central electrostatic interactions, and the inner electrons can be treated as a deformable core of charge. In this case the term energy T (appropriately averaged over magnetic fine structure and spin multiplicity) can be represented by [1]

$$T_{nl} = TH_{nl} + A\langle r^{-4}\rangle_{nl} + B\langle r^{-6}\rangle_{nl}. \tag{8}$$

Here TH and $\langle r^{-s}\rangle$ are the term energy and radial expectation values for a corresponding hydrogenlike ion. A plot of the empirical quantity $(T-TH)/\langle r^{-4}\rangle$ vs $\langle r^{-6}\rangle/\langle r^{-4}\rangle$ for various n and l often yields a straight line indicating that A and B are approximately constant for a given atomic ion. For an ideally nonpenetrating case these quantities could be theoretically computed as $A = \alpha_d$ and $B = \alpha_q - 6\beta$ where α_d and α_q are the dipole and quadrupole polarisabilities of the core and β is a nonadiabatic correction for the inability of the core to instantaneously adjust to the motion of the orbital electron.

The specification of A and B predictively systematises the ionisation energies of all states of sufficiently high n and l in a given ion. If a chain of accurately measured transitions connecting the nonpenetrating states to the ground state is available, this can be used to specify the ionisation potential of the cold ion. Thus high Rydberg states provide a valuable means for determining both the ionisation potential of the atomic ion in question and the electrostatic polarisabilities of its next higher stage of ionisation.

Unfortunately the condition of nonpenetrating orbitals is not completely met in much of the data presently available. Generally, theoretical calculations and empirical values agree well for A, but disagree in both magnitude and sign for B. For measurements of insufficiently high n and l, penetration effects have been shown [1] to be approximately constant for fixed l, and tend to affect empirical values of B more than those of A. Thus the polarisation model can yield reliable predictions for the energies within each separate Rydberg series of an ion, despite the penetration distortions in the effective polarisation parameters. The electric fields inherent in spark spectroscopy Stark-quench states of very high l, so low density sources such as beam foil excitation are necessary to obtain values for the undistorted polarisabilities.

Extensive studies have been made of polarisabilities for the Ne isoelectronic sequence both by ab initio theory and by empirical use of the core polarisation model to specify the spectra of high Rydberg states in the Na isoelectronic sequence. Theoretical values for both α_d and α_q have been computed by the relativistic random phase approximation through $Z = 92$ by Johnson *et al.* [52], but theoretical values for β are virtually nonexistent. Empirical values for A and B have been deduced by Edlén [53] [in the notation A(Edlén) $= \zeta^4 A$ and k(Edlén) $= \zeta^2 B/A$], who also produced explicit extrapolation formula for these quantities. Edlén's data reduction for higher Z is primarily based on nf states, which contain penetration effects that distort them from the values of Ref. [52]. Figure 7 traces the theoretical values for α_d (solid line), α_q (dashed line), and the empirical values for A(+) and B(○). The extrapolations of A and B to high Z are indicated by dotted lines. Although the theoretical and

empirical values do not coincide, their trends are similar, suggesting that the penetration distortions also vary smoothly with Z. Thus it can reasonably be assumed that the extrapolation formulae of Edlén will accurately predict the nf term energies for all Z, although they should not be used for higher values of l.

Recent published spectroscopic analyses now permit the use of the Edlén's A and B values to determine ground state ionisation potentials throughout the Na sequence. Spectroscopic analysis is essentially complete for the ions Na I–Cl VII [28–33]. Precision measurements are available for most of the $3s$–$3p$, $3p$–$3d$, and $3d$–$4f$ transition wavelengths for the ions Ar VIII–Sn XXXX (as reported and summarised in Ref. [34]). Furthermore, Reader *et al.* [34] have parametrised the differences between the observations and corresponding Dirac–Fock calculations, and produced a set of smoothed values for Ar VIII–Xe XXXXIV that are expected to be accurate to within ± 0.07 Å.

We have deduced ground state ionisation potentials for the Na sequence, using the polarisation model and Edlén's A and B values to establish $4f$ ionisation potentials, and using the published $3s$–$3p$–$3d$–$4f$ transition wavelengths to establish the $4f$ excitation energies. This permitted the determination of all ionisation potentials through Xe^{43+}. To extend this further, we computed the corresponding quantities using the MCDF code, then semiempirically parametrised the differences between empirical and theoretical values, and finally extrapolated these differences to obtain predicted ionisation potentials through $Z = 92$ [74]. The results of this analysis are quoted in Table IV.

In the next section, methods will be described whereby information concerning excitation energies, ionisation potentials, and core polarisabilities obtained from spectroscopic wavelength data in this manner can be used to make reliable predictions concerning transition rates.

Table IV. *Ionisation potentials for the Na isoelectronic sequence [74] (cm^{-1})*

Z	$T(4f)$[a]	$3s$–$4f$[b]	IP
30	2 752 213	3 195 113	5 947 326
31	3 034 356	3 476 909	6 511 265
32	3 330 273	3 771 013	7 101 287
33	3 639 970	4 077 257	7 717 227
34	3 963 451	4 396 031	8 359 481
35	4 300 718	4 727 036	9 027 754
36	4 651 779	5 069 231	9 721 010
37	5 016 637	(5 424 937)	10 441 573
38	5 395 297	5 793 243	11 188 540
39	5 787 764	6 173 336	11 961 100
40	6 194 046	6 567 032	12 761 077
41	6 614 146	6 975 631	13 589 777
42	7 048 073	7 397 926	14 445 999
43	7 495 831	(7 831 618)	15 327 450
44	7 957 429	8 279 778	16 237 208
45	8 432 872	(8 734 004)	17 166 876
46	8 922 169	(9 217 283)	18 139 451
47	9 425 324	(9 707 603)	19 132 927
48	9 942 349	(10 211 679)	20 154 028
49	10 473 249	(10 730 538)	21 203 787
50	11 018 033	11 267 148	22 285 181
51	11 576 709	(11 813 335)	23 390 044
52	12 149 287	(12 377 476)	24 526 763
53	12 735 772	(12 957 024)	25 692 796
54	13 336 178	(13 552 590)	26 888 768
74	28 283 008		57 523 696[c]
79	32 900 716		67 523 825[c]
90	44 314 691		92 880 985[c]
92	46 576 595		98 220 914[c]

[a] Term values obtained from the core polarisation model using effective polarisabilities obtained from the formulae of Edlén [53].

[b] Excitation energies obtained from measured $3s$–$3p$–$3d$–$4f$ wavelengths in Ref. [34]. Parentheses indicate values interpolated and extrapolated in Ref. [34] using a parametrisation of the difference between observed and MCDF wavelength values.

[c] Our extrapolation through a parametrisation of the difference between the ionisation limits deduced from observations and those computed by MCDF.

7. Semiempirical specification of transition probabilities using wavelength data

Lifetimes of the ns–np resonance transitions in alkalilike isoelectronic sequences provide a challenging confrontation between theory and experiment. Although these systems consist basically of a single electron outside a closed shell, the intrashell nature of these transitions produces both theoretical and experimental subleties. The relative positions of the levels has a strong isoelectronic variation, and the regular doublet interval increases relative to the irregular doublet interval with increasing ionicity. This causes lifetimes and state populations of the individual fine structure levels to have a similarly strong isoelectronic variation. Theoretically, core polarisation and other types of electron correlation, spin–orbit coupling and other relativistic interactions, and the advantages of Breit–Pauli and fully relativistic treatments can vary with the degree of ionicity. Experimentally, these intrashell decay channels are repopulated by faster extrashell cascades and by the yrast chain, so experimental decay curves exhibit both growing-in and growing-out cascades. Lifetime determinations by simple multiexponential fitting procedures are known to be unreliable for these systems [54, 55] and more sophisticated experimental procedures must be used [56, 57].

An uncritical compilation of lifetime data for np lifetimes in alkalilike sequences can be misleading, since early measurements based solely on exponential curve fitting systematically overestimated the lifetimes. Analyses that fit a sum of exponential functions to the decay curve of a heavily cascaded alkalilike resonance transition almost invariably yield an overestimate of the lifetime [54, 55] and such data should be categorically excluded from comparisons with theory. The tendency of the ns–np experimental lifetimes to exceed theoretical estimates has sometimes been attributed entirely to cascade repopulation, but it now appears that discrepancies toward longer lifetimes still persist after cascade effects have been eliminated.

Precision lifetime measurements can be made by methods that are free of problems due to cascade repopulation. One method involves selective excitation of a fast ion beam by a laser. Gaupp *et al.* [58] have performed high precision ($< 0.2\%$) beam-laser measurements for the $J = 1/2$–$1/2$ resonance transitions in Li I and Na I which yielded lifetimes that are several experimental standard deviations longer than those predicted by *ab initio* theory. Hyperfine quantum beats prevented a precise measurement for the $J = 1/2$–$3/2$ resonance transitions with the geometry employed in Ref. [58]. However, a measurement of the ratio of the $3s$–$3p$ line strengths for Na I by Gawlik *et al.* [59] (using differential

Faraday rotation) yielded 1.983 ± 0.004, and this permits precise specification of the lifetimes of both $3p$ levels. These measurements produced troubling discrepancies with theory [60–64], and concern has been expressed [62] as to whether calculational uncertainties can accommodate the differences.

The only source of direct lifetime measurements for highly ionised atomic systems is by foil excitation of a fast ion beam, which is nonselective. While beam-foil techniques do not yet permit measurements to within parts per thousand for highly ionised systems, methods are available that provide internal tests which insure that quoted uncertainties (nominally 5%) are realistic. Recent measurements have utilised the ANDC (arbitrarily normalised decay curve) method [56, 57] which exploits dynamical correlations among cascade-related decay curves to reliably extract lifetimes. This method utilises the rate equation connecting the population of the nth level to those of the i levels that cascade directly into it. Since the instantaneous time dependence of each level population is, to within constant factors involving the transition probabilities and detection efficiencies, proportional to the measured decay curve $I_{ik}(t)$, the instantaneous population equation can be written

$$\tau_n \mathrm{d}I_{nf}/\mathrm{d}t = \Sigma_i E_{in} I_{in}(t) - I_{nf}(t). \quad (9)$$

This provides the exposition of a set of relationships between a given time point on the primary decay curve and the corresponding points on its direct cascades, with constant coefficients given by the lifetime τ_n and the relative normalisation parameters E_{in}. Analysis consists of using this equation to relate measured $I_{jk}(t)$'s (using numerical differentiation or integration) to determine τ_n and the E_{in}'s through a linear regression. If all significant direct cascades have been included, the goodness-of-fit will be uniform for all time subregions, but if important cascades have been omitted or blends are present, the fit will vary over time subregions. For alkalilike resonance transitions, the dominant cascading along the yrast chain is completely specified by the p–d channel. Rugged ANDC algorithms have been developed [65, 66], which contain analyses of the propagation and correlation of errors [67].

A series of beam-foil measurements for the $3s$–$3p$ and $3p$–$3d$ decay curves in the Na sequence that extracts lifetimes by the ANDC method has been reported, and these comprise the data base against which theoretical calculations should be compared. This has been done in Ref. [74], as shown in Fig. 8 which plots level and multiplet absorption oscillator strengths vs reciprocal nuclear charge. The measurements were performed separately for each fine structure component to typically 5% accuracies, and include the ions S VI [68], Cl VII [69], Ar VIII [70], Ti XII [71], Fe XVI [71, 72], Ni XVIII [71] and Cu XIX [71]. Earlier measurements which utilised only curve fitting methods or determined only multiplet values may contain systematic errors which exceed quoted uncertainties and have not been included here. MCDF calculations [61] are indicated (* for level, + for multiplet), and clearly overestimate the oscillator strength (hence underestimate the lifetime). Nonrelativistic MCHF calculations [60] agree reasonably well, but are available only for the multiplet value and for $Z \leqslant 26$. The solid curves trace our semiempirical Hartree–Slater calculations [74], which make use of spectroscopic wavelengths, ionisation potentials, and core polarisabilities, and will be discussed in more detail below.

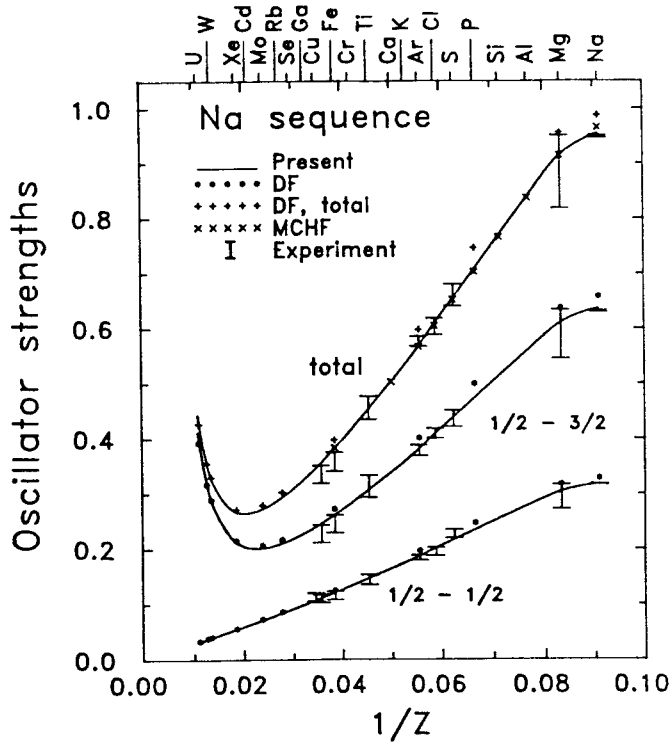

Fig. 8. Experimental and theoretical values for the line and multiplet absorption oscillator strengths vs reciprocal nuclear charge for the Na isoelectronic sequence. Points within error bars indicate measurements that exclude of properly account for cascades; solid lines trace Hartree–Slater semiempirical computations [74]. (*, +) denote MCDF calculations [61], and (×) denotes MCHF calculations [60].

Many types of calculations have been made for the Na sequence, but each has limitations. Ab initio MCDF calculations [61] treat the fine structure in a fully relativistic manner, but do not adequately describe correlation effects. Nonrelativistic MCHF calculations [60] include electron correlation, but yield only a multiplet line strength, and compromise their ab initio nature by using experimental wavelengths to obtain level lifetimes. Semiempirical calculations using the Coulomb approximation sometimes yield striking agreement with experiment, but they are not *ab initio*, require spectroscopic data as input, and do not describe the inner portion of the wave function.

A difficulty in selecting between a fully relativistic treatment without electron correlation and a nonrelativistic treatment with correlation is shown in Fig. 9. Here theoretical values for the line strength ratio $S(1/2, 3/2):S(1/2, 1/2)$ for the $3s$–$3p$ transition in the Na sequence are plotted versus nuclear charge. The nonrelativistic limit of this ratio is exactly two and independent of Z, which yields a wavelength-cubed dependence for the ratio of the lifetimes of the fine structure levels. For low Z this is nearly true, and the deviation from two is less than 1% for elements through the iron group. (The ratio is 1.983 for Na I, but exceeds two for all other members of the sequence.) For higher Z the ratio becomes strongly Z dependent, and exceeds two by 15% for $Z > 80$. Thus for Na-like ions beyond the iron group, relativistic corrections to both the wavelength and the line strength are necessary.

The Hartree–Slater semiempirical approach [73, 74] involves the integration of the Schrödinger equation with a realistic model potential, constrained to yield the experimental binding energy. The model potential includes the single electron central field, the spin–orbit interaction, and

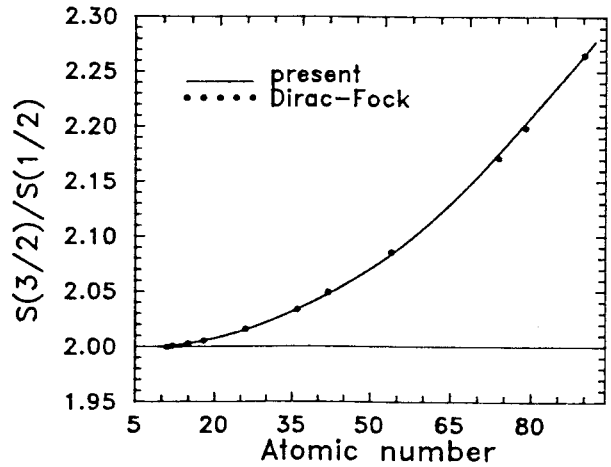

Fig. 9. Plot of the ratio of theoretical line strengths vs nuclear charge for the two $3s$–$3p$ fine structure transitions in the Na isoelectronic sequence. The solid line denotes Hartree–Slater semiempirical calculations and the solid circles denote MCDF calculations. For $Z < 30$ the ratio is with 1% of the nonrelativistic value 2, but for large Z the ratio exceeds 2 by measurable amounts [74].

the core polarisation potential (as specified by the empirical dipole polarisability), and the specification of the binding energy requires input values for both the excitation energies and the ionisation limit. The large data base now available for the Na sequence and the ionisation potential determination given in Table IV permits the calculations shown in Fig. 8.

Measurements for both the $4s$–$4p$ and $4p$–$4d$ resonance transitions in the Cu isoelectronic sequence that employ the ANDC method for extraction of lifetimes provides another data base which can be compared with *ab initio* and semiempirical calculations. Figure 10 presents a plot of the oscillator strengths f vs $1/Z$ for the Cu sequence. The experimental values (points with error bars) included here were obtained by the ANDC method for Zn II [77], Ga III [78] Ge IV [79], As V [80], Se VI [81], Kr VIII [82, 83] and I XVV [84], and by non-ANDC measurements that paid special attention to cascade corrections for Cu I [75] and Mo XIV [83]. The theoretical calculations included are denoted: relativistic methods [85] (*); nonrelativistic MCHF with polarisation corrections [86] (×); numerical Coulomb approximation [89] (○); and our Hartree–Slater semiempirical calculations [90] (solid lines).

The Hartree–Slater calculations require spectroscopic data. Comprehensive published spectroscopic analyses have established the $n = 4$ energy levels and the ionisation potentials for all Cu-like ions (except Tc) up to Sn^{21+}, and similar analyses are available for selected ions from Ba^{27+} to W^{74+} [12]. Wavelength measurements are available for both fine structure lines of the $3s$–$4p$ resonance multiplet for Au^{52+}, Pb^{55+} and Bi^{56+}, and for the $J = 1/2$–$3/2$ lines for Th^{61+} and U^{64+}. The $4p$ fine structure splitting has been semiempirically parametrised by the method of Fig. 2 for all ions in the sequence. Theoretical dipole and quadrupole polarisabilities for the Ni-like cores have been published [52] for a closely spaced set of ions through U^{64+}, which we have interpolated [90]. To complete the required data set it was necessary only to interpolate the 1/2–1/2 resonance transition wavelength and to extrapolate the ionisation potential, which was done [91] by parametrising the differences between observed values and MCHF calculations.

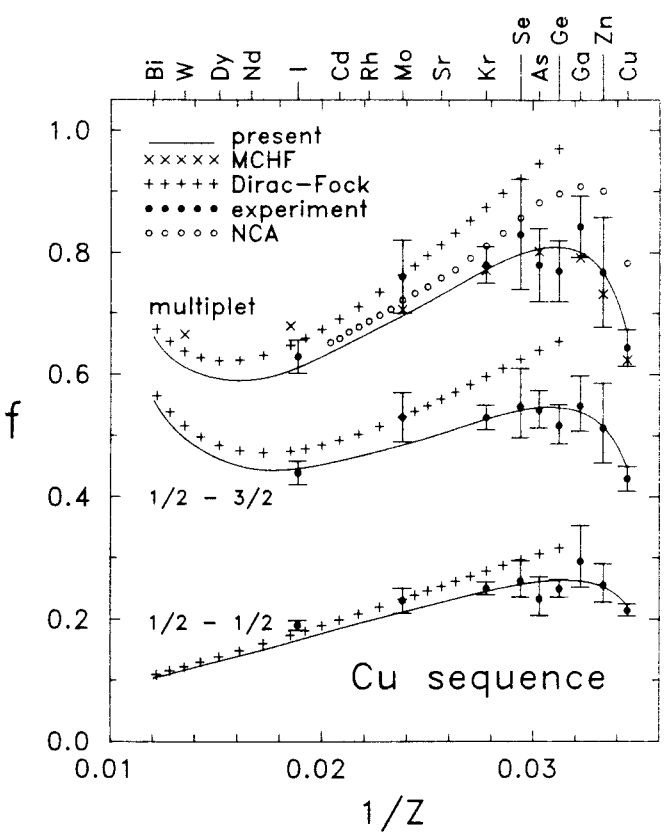

Fig. 10. Experimental and theoretical values for the line and multiplet absorption oscillator strengths vs reciprocal nuclear charge for the Cu isoelectronic sequence. Points within error bars indicate measurements that exclude of properly account for cascades; solid lines trace Hartree–Slater semiempirical computations [90]. (*, +) denotes MCDF calculations [86], and (×) denotes MCHF calculations [85].

These data were used as inputs to the Hartree–Slater program and produced the results [91] presented in Fig. 10.

The systematisation described here brings three methods to bear upon transition probability specification. The Hartree–Slater method seems to provide very accurate predictions of transition probabilities, but requires spectroscopic data. If comprehensive wavelength measurements are not available, existing data can be semiempirically parametrised and extrapolated. This extrapolation can be aided by ab initio spectroscopic calculations, if the *ab initio* trends are of the type illustrated in Fig. 1(b). In this manner, *ab initio* energy level calculations can be semiempirically adjusted to match experimental trends, then inserted into the Hartree–Slater program to produce semiempirical wave functions which yield transition rates of quality that is superior to that obtained by fully *ab initio* methods.

Acknowledgements

I am grateful to Professors David Ellis and Constantine Theodosiou for valuable suggestions, and to Drs Lars Engström, Roger Hutton and Elmar Träbert for providing access to new measurements prior to publication. The work was supported by the US Department of Energy, Division of Chemical Sciences, Office of Basic Energy Sciences, under contract number DE AS05 80ER10676.

References

1. Edlén, B., Handb. Physik, Vol. XXVII, Springer, Berlin, (1964) pp. 80–220; Curtis, L. J., Physica Scripta **35**, 805 (1987).

2. Grant, I. P., McKenzie, B. J., Norrington, P. H., Mayers, D. F. and Pyper, N. C., Comput. Phys. Commun. **21**, 207 (1980).
3. Curtis, L. J., J. Phys. **B10**, L641 (1977).
4. Curtis, L. J., J. Phys. **B18**, L651 (1985); **B19**, 1699 (1986) E.
5. Garcia, J. D. and Mack, J. E., J. Opt. Soc. Am. **55**, 654 (1965).
6. Drachman, R. J., Phys. Rev. **A26**, 1228 (1982).
7. Erickson, G. W., J. Phys. Chem. Ref. Dat. **6**, 831 (1977).
8. Douglas, M., Phys. Rev. **A6**, 1929 (1972).
9. Malvetti, M., Phys. Rev. **A35**, 1490 (1987).
10. Cheng, K. T. and Wagner, R. W., Phys. Rev. **A36**, 5435 (1987).
11. Curtis, L. J., Nucl. Instr. Meth. in Phys. Res. **B31**, 146 (1988).
12. Reader, J. and Luther, G., Physica Scripta **24**, 732 (1981).
13. Reader, J., Acquista, N. and Cooper, D., J. Opt. Soc. Am. **73**, 1765 (1983).
14. Seely, J. F., Ekberg, J. O., Brown, C. M., Feldman, U., Behring, W. E., Reader, J. and Richardson, M. C., Phys. Rev. Lett. **57**, 2924 (1986).
15. cf. Curtis, L. J., J. Phys. **B14**, 631 (1981).
16. Isberg, B. and Litzén, U., Physica Scripta **31**, 533 (1985).
17. Joshi, Y. N. and van Kleef, Th. A. M., Physica Scripta **34**, 135 (1986).
18. Trigueiros, A., Pettersson, S. G. and Reyna Almandos, J. G., Physica Scripta **34**, 164 (1986).
19. Churilov, S. S., Ryabtsev, A. N. and Wyart, J.-F., Physica Scripta **38**, 326 (1988).
20. Reader, J., Acquista, N. and Goldsmith, S., J. Opt. Soc. Am. **B3**, 874 (1986).
21. Curtis, L. J., Reader, J., Goldsmith, S., Denne, B. and Hinnov, E., Phys. Rev. **A29**, 2248 (1984).
22. Rahimullah, K., Chaghtai, M. S. Z. and Khatoon, S., Physica Scripta **18**, 96 (1978).
23. Hansen, J. E. and Persson, W., J. Opt. Soc. Am. **64**, 696 (1974).
24. Persson, W. and Wahlström, C.-G., Physica Scripta **30**, 169 (1984).
25. cf. Curtis, L. J. and Ramanujam, P. S., Physica Scripta **27**, 417 (1983).
26. Curtis, L. J. and Silbar, R. R., J. Phys. **B17**, 4087 (1984).
27. Curtis, L. J., Phys. Rev. **A35**, 2089 (1987).
28. Risberg, P., Arkiv Fysik **10**, 583 (1956); **9**, 483 (1955).
29. Isberg, B., Arkiv Fysik **35**, 551 (1968).
30. Toresson, Y. G., Arkiv Fysik **17**, 179 (1960).
31. Magnusson, C. E. and Zetterberg, P. O., Phys. Scripta **10**, 177 (1974).
32. Joelsson, I., Zetterberg, P. O. and Magnusson, C. E., Physica Scripta **20**, 145 (1979).
33. Jupén, C. and Fremberg, J., Physica Scripta **30**, 260 (1984).
34. Reader, J., Kaufman, V., Sugar, J., Ekberg, J. O., Feldman, U., Brown, C. M., Seely, J. F. and Rowan, W. L., J. Opt. Soc. Am. **B4**, 1821 (1987).
35. cf. Curtis, L. J. and Ramanujam, P. S., J. Opt. Soc. Am. **73**, 979 (1983).
36. cf. Curtis, L. J. and Ramanujam, P. S., Physica Scripta **27**, 417 (1983).
37. cf. Smitt, R., Svensson, L. A. and Outred, M., Physica Scripta **13**, 293 (1976).
38. Denne, B., Hinnov, E., Suckewer, S. and Cohen, S., Phys. Rev. **A28**, 206 (1983).
39. Suckewer, S., Hinnov, E., Cohen, S., Finkenthal, M. and Sato, K., Phys. Rev. **26**, 1161 (1982).
40. Hinnov, E., in "Atomic Physics of Highly Ionized Atoms", (Edited by R. Marrus), Plenum Pub. Corp (1983).
41. Curtis, L. J., J. Opt. Soc. Am. **B2**, 407 (1985); **B3**, 177 (1986); **B3**, 1102 (1986).
42. Edlén, B., Solar Physics **24**, 356 (1972).
43. Johnson, W. R., Blundell, S. A. and Sapirstein, J., Phys. Rev. **A37**, 2764 (1988).
44. Edlén, B., Physica Scripta **19**, 255 (1979).
45. Hinnov, E., Astrophys. J. **230**, L197 (1979).
46. Hinnov, E., Boody, F., Cohen, S., Feldman, U., Hosea, J., Sato, K., Schwob, J. L., Suckewer, S. and Wouters, A., J. Opt. Soc. Am. **B3**, 1288 (1986).
47. Denne, B. and Hinnov, E., Physica Scripta **35**, 811 (1987).
48. Hinnov, E., Ramsey, A., Stratton, B., Cohen, S. and Timberlake, J., J. Opt. Soc. Amer. **B4**, 1293 (1987).
49. Denne, B., Hinnov, E., Ramette, J. and Saoutic, B., personal communication.
50. Mohr, P. J., Ann. Phys. (NY) **88**, 26; 52 (1974); Phys. Rev. **A26**, 2338 (1982).
51. Johnson, W. R. and Soff, G., Atomic Data Nucl. Data Tables **33**, 405 (1985).
52. Johnson, W. R., Kolb, D. and Huang, K.-N., Atom. Data Nucl. Data Tables **28**, 333 (1983).
53. Edlén, B., Physica Scripta **17**, 565 (1978).
54. Crossley, R. J. S., Curtis, L. J. and Froese Fischer, C., Phys. Lett. **57A**, 220 (1976).
55. Younger, S. M. and Wiese, W. L., Phys. Rev. **A18**, 2366 (1978).
56. Curtis, L. J., Berry, H. G. and Bromander, J., Phys. Lett. **34A**, 169 (1971).
57. Curtis, L. J., in "Beam-Foil Spectroscopy," (Edited by S. Bashkin), pp. 63–109. Springer-Verlag (1976).
58. Gaupp, A., Kuske, P. and Andrä, H. J., Phys. Rev. **A26**, 3351 (1982).
59. Gawlik, W., Kowalski, J., Neumann, R., Wiegemann, H. B. and Winkler, K., J. Phys. **B12**, 3873 (1979).
60. Froese Fischer, C., Can. J. Phys. **54**, 1465 (1976).
61. Kim, Y.-K. and Cheng, K.-T., J. Opt. Soc. Am. **68**, 836 (1978).
62. McEachran, R. P. and Cohen, M., J. Phys. **B16**, 3125 (1983).
63. Biémont, E., Physica **85C**, 393 (1977).
64. Karwowski, J. and Szulkin, M., J. Phys. **B14**, 1915 (1981); Shevelko, V. P., Opt. Spectrosk. **36**, 7 (1974); Laughlin, C., Lewis, M. N. and Horak, Z. J., Astrophys. J. **197**, 799 (1975).
65. Engström, L., Nucl. Instr. Meth. **202**, 369 (1982).
66. Weckström, K., Phys. Scripta **23**, 849 (1981).
67. Pinnington, E. H. and Gosselin, R. N., J. Physique (Paris) **40**, C1-149 (1979).
68. Ekberg, J. O., Engström, L., Bashkin, S., Denne, B., Huldt, S., Johansson, S., Jupén, C., Litzén, U., Trigueiros, A. and Martinson, I., Physica Scripta **27**, 425 (1983).
69. Jupén, C., Engström, L., Huldt, S., Trigueiros, A., Ekberg, J. O., Litzén, U. and Martinson, I., Physica Scripta **29**, 226 (1984).
70. Reistad, N., Engström, L. and Berry, H. G., Physica Scripta **34**, 158 (1986).
71. Hutton, R., Engström, L. and Träbert, E., Phys. Rev. Lett. **60**, 2469 (1988).
72. Buchet, J. P., Buchet-Poulizac, M. C., Denis, A., Desesquelles, J. and Druetta, M., Phys. Rev. **A22**, 2061 (1980).
73. Theodosiou, C. E., Phys. Rev. **A30**, 2881 (1984).
74. Theodosiou, C. E. and Curtis, L. J., Phys. Rev. **A38**, 4435 (1988).
75. Hannaford, P. and McDonald, D. C., J. Phys. **B11**, 1177 (1978).
76. Rambow, F. H. K. and Shearer, L. D., Phys. Rev. **A14**, 1735 (1976).
77. Martinson, I., Curtis, L. J., Huldt, S., Litzén, U., Liljeby, L., Mannervik, S. and Jelenkovic, B., Physica Scripta **19**, 17 (1979).
78. Ansbacher, W., Pinnington, E. H., Bahr, J. L. and Kernahan, J. A., Can. J. Phys. **63**, 1330 (1985).
79. Pinnington, E. H., Bahr, J. L. and Irwin, D. J. G., Phys. Lett. **A84**, 247 (1981).
80. Pinnington, E. H., Bahr, J. L., Kernahan, J. A. and Irwin, D. J. G., J. Phys. **B14**, 1291 (1981).
81. Bahr, J. L., Pinnington, E. H., Kernahan, J. A. and O'Neill, J. A., Can. J. Phys. **60**, 1108 (1982).
82. Pinnington, E. H., Gosselin, R. N., O'Neill, J. A., Kernahan, J. A., Donnelly, K. E. and Brooks, R. L., Physica Scripta **20**, 151 (1979).
83. Livingston, A. E., Curtis, L. J., Schectman, R. M. and Berry, H. G., Phys. Rev. **A21**, 771 (1980).
84. Denne, B. and Poulsen, O., Phys. Rev. **A23**, 1229 (1981).
85. Johnson, B. M., Jones, K. W., Gregory, D. C., Ekberg, J. O., Engström, L., Kruse, T. H. and Cecchi, J. L., Physica Scripta **32**, 210 (1985).
86. Cheng, K.-T. and Kim, Y.-K., Atom. Data Nucl. Data Tables **22**, 547 (1978).
87. Froese Fischer, C., J. Phys. **B10**, 1241 (1977).
88. Migdałek, J. and Bayliss, W. E., J. Phys. **B12**, 1113 (1979).
89. Weiss, A. W., J. Quant. Spectrosc. Radiat. Transfer **18**, 481 (1977).
90. Lindgård, A., Curtis, L. J., Martinson, I. and Nielsen, S. E., Physica Scripta **21**, 47 (1980).
91. Curtis, L. J. and Theodosiou, C. E., Phys. Rev. **A**, (in press).